Latin American Journal of Solids and Structures
www.lajss.org

# Experimentally Validated Combustion and Piston Fatigue Life Evaluation Procedures for the Bi-Fuel Engines, Using an Integral-Type Fatigue Criterion

**Abstract**

A relatively complete procedure for high cycle fatigue life assessment of the engine components is outlined in the present paper. The piston is examined as a typical component of the engine. In this regard, combustion process and transient heat transfer simulations, determination of the instantaneous variations of the pressure and temperature in the combustion chamber, kinematic and dynamic analyses of the moving parts of the engine, thermoelastic stress analyses, and fatigue life analyses are accomplished. Results of the simulation are compared with the test data to verify the results. The heat transfer results are validated by the experimental results measured by the Templugs. The nonlinear multipoint contact constraints are modeled accurately. Results of the more accurate available fatigue criteria are compared with those of a fatigue criterion recently proposed by the first author. These results are also evaluated by comparing them with the experimental durability tests. The presented procedure may be used, e.g., to decide whether it is suitable to convert a gasoline-based engine to a bi-fuel one. Results of the various thermomechanical fatigue analyses performed reveal that the piston life decreases considerably when natural gas is used instead of gasoline.

**Keywords**

Heat transfer and combustion simulation; Engine; Piston; Fatigue failure; Experimental results.

M. Shariyat [a *]
J. Fathi Sola [b]
S.A. Jazayeri [c]

[a*] Professor, Faculty of Mechanical Engineering, K.N. Toosi University of Technology, Tehran, Iran.
Email: m_shariyat@yahoo.com
(Corresponding author)
[b] Ph.D. Candidate, Faculty of Mechanical Engineering, K.N. Toosi University of Technology, Tehran, Iran.
Email: jalalfathi@gmail.com
[c] Associate Professor, Faculty of Mechanical Engineering, K.N. Toosi University of Technology, Tehran, Iran.
Email: Jazayeri@kntu.ac.ir

http://dx.doi.org/10.1590/1679-78251937

Received 21.02.2015
In revised form 15.01.2016
Accepted 19.02.2016
Available online 27.02.2016

## 1 INTRODUCTION

Accuracy of the employed design procedure may affect the size, cost, and durability of the resulting mechanical assemblies. Due to various aspects of the internal combustion engines, the combustion, heat transfer, mechanism, stress, and fatigue failure analyses have often been treated in separate

packages. However, a complete knowledge about these analyses may lead to an integrated and optimized design. On the other hand, due to some fuel resources management programs, some researchers have proposed using the natural gas, e.g. in the form of compressed natural gas (CNG), as an alternative fuel. Due to different combustion characteristics, employing different fuels in the gasoline-based engines leads to some side effects such as performance degradation, increase in the thermal losses, emission, and lower fatigue lives for the components. Piston as a key component of the engine that is vulnerable to severe cyclic and transient thermal and mechanical loads can directly be affected by the mentioned conversion (Shariyat and Djamshidi 2009).

While some researchers modeled the combustion process (Kajiwara 2002), some researchers have investigated the thermoelastic stresses caused by the combustion process. Ivaschenko et al. (1980) studied the stresses in a piston of a diesel engine. They employed an analytical method on the basis of solving Laplace's equation to determine the von Mises stresses in specific regions of the piston, assuming a quasi-static condition. Valdes et al. (2001) performed velocity, acceleration, and finite element transient thermal and stress analyses for the piston. Some researches were devoted to fatigue life assessment under thermomechanical loads. Su et al. (2002) performed a thermoelastic high cycle fatigue and creep analysis in ABAQUS for the engine cylinder head and validated their stress analysis results by means of some installed strain gauges. Silva (2006) analyzed the thermomechanical damage fatigues in the pistons. He stated that the wear, temperature gradient, and fatigue-related phenomena are the main origins of the pistons damages and reported that the regions located at the pin holes, piston crown, grooves and skirt, are more critical. A finite element linear static analysis, using COSMOS was used for stress and temperature determination during the combustion.

In the present paper, a complete algorithm for design of the engine components against the fatigue failure is presented based on simulation of the combustion, heat transfer, kinematic, dynamic, and thermoelastic stress analyses. Eventually, the mentioned algorithm is employed for evaluating effects of converting a gasoline-based engine to a bi-fuel one on the fatigue life of the piston under the combustion thermomechanical loads. The combustion model presented previously by Jazayeri and his co-authors (Ghazi Mir Saied et al. 2006; Shahangian et al. 2007; Mohammadi et al. 2008; Jahanian and Jazayeri 2009) is enhanced and employed to model the combustion process for the two mentioned fuels. Based on the determined combustion pressures, temperatures and the non-uniform convection heat transfer coefficients, the combustion thermomechanical loads, the piston pin load, and the frictional and inertia forces are computed for the gasoline and the natural gas engines. In the stress analysis stage, higher-order Lagrangian elements are adopted to avoid stress discontinuity in the mutual boundaries of the elements. While some of the available fatigue theories have mainly been proposed to check whether or not a component has an infinite life, some other theories, such as the most widely used Fatemi-Socie (1988) and Swith-Watson-Topper (1970) models have been proposed for fatigue life prediction purposes. In the present research, the fatigue lives are predicted based on the fatigue criteria proposed recently by Shariyat (2008; 2009a,b; 2010). The fatigue lives are computed based on simulation of the standard durability tests, at the critical region of the piston. Various engineering softwares have been used to extract the CAE and theoretical results. Finally, the temperatures, pressures, and the fatigue lives are compared with the experimental ones.

## 2 SIMULATION OF THE COMBUSTION PROCESS

Accurate modeling of the combustion process is a key issue for comparing performances of the gasoline and bi-fuel engines and consequently, estimation of the fatigue lives. In this regard, the combustion is modeled for an inline four-cylinder spark-ignited (SI) gasoline-based engine. The relevant engine information is listed in Table 1. Among the traditional models, the more accurate open system model which covers all the stages is employed to model the combustion process.

Information of the gasoline and the natural gas is given in Table 2. The combustion equations of the gasoline ($C_{8.26}\ H_{15.5}$) and the compact natural gas (CNG) in the stoichiometric condition are as follows:

$$\begin{cases} \text{CNG}+x\,(O_2+3.76\,N_2\,) \rightarrow 1.0453\,CO_2+3.9616/2\ H_2O+x*3.76\,N_2 \\ x=1.0453+3.9616/4+.02=2.0157 \\ [AF]_{molar}=2.0157(1+3.76)=9.595 \\ [AF]_{mass}=15.27 \end{cases} \tag{1}$$

$$\begin{cases} C_{8.26}\ H_{15.5}+12.135(O_2+3.76\,N_2) \rightarrow 8.26\,CO_2+15.5/2\ H_2\ O+45.6276\,N_2 \\ [AF]_{molar}=12.135(1+3.76)=57.76 \\ [AF]_{mass}=14.1 \end{cases} \tag{2}$$

where $[AF]_{molar}$ and $[AF]_{mass}$ represent the molar and mass air-fuel ratios, respectively.

| Quantity | value |
|---|---|
| Cylinder diameter | 78.6 mm |
| Stroke | 85 mm |
| Connecting rod length | 134.5 mm |
| Piston eccentricity | 0.8 mm |
| Compression ratio | 11 |
| Cylinder volume | 1650 cc |
| Maximum RPM | 6000 RPM |
| Distance between the piston pin and the C.G. of the connecting rod | 40.9 mm |
| Engine cylinder head heat transfer area | 6800 $mm^2$ |
| Piston mass | 0.317 kg |
| Connecting rod mass | 0.5 kg |
| Inertia moment of the connecting rod | 0.001738 $kg.m^2$ |
| Height of the piston | 51.7 mm |
| Location of the piston hole relative to the top surface | 29.7 mm |

**Table 1**: Specifications of the considered engine.

A two zone Wiebe function is used to simulate the combustion. Crank angles corresponding to the combustion initiation and the maximum pressure are measured experimentally and given in Table 3. Since a full fatigue analysis requires an accurate full time history of the applied thermomechanical loads, the combustion process is simulated for different RPMs. The real to stoichiometric fuel ratios measured through experiments using results of the combustion analysis (Eqs. 1 and 2) are given in Table 4 for different RPMs. It is known that the stoichiometric or theoretical combustion is an ideal combustion process wherein the fuel is burned completely. Results of Table 4 reveal that results of the stoichiometric calculations of the CNG (Eq. 1) are almost coincident with the real ones and to some extent, independent of the RPM of the engine whereas results of the gasoline (Eq. 2), are dependent on the RPM so that in high RPMs, amount of the unburned fuel, soot, smoke, and carbon monoxide increase.

| Fuel type | Chemical formula | Molecular weight | $Q_{LHV}\, Mj/kg$ |
|---|---|---|---|
| Gasoline | $C_{8.26}\, H_{15.5}$ | 114.82kg | 44 |
| Natural gas | $C_{1.0453}\, H_{3.9616}\, O_{0.02}\, N_{0.09}$ | 18.13 kg | 44.98 |

**Table 2**: Information of the gasoline and the natural gas. $Q_{LHV}$ is the low heating value of the reference fuels.

| Engine RPM | Ignition advance (BTDC) | | Maximum pressure angle (ATDC) | |
|---|---|---|---|---|
| | Gasoline | Natural gas | Gasoline | Natural gas |
| 2000 | 5 | 23 | 32 | 14 |
| 3500 | 15 | 26 | 19.5 | 11 |
| 6000 | 14 | 31 | 21 | 8 |

**Table 3**: The measured crank angles corresponding to the combustion initiation and the maximum pressure at the full load condition (Heywood 1988).

| Engine RPM | Natural gas | Gasoline |
|---|---|---|
| 1250 | 0.962 | 0.895 |
| 1500 | 0.962 | 0.9 |
| 2000 | 0.968 | 0.9 |
| 2500 | 0.965 | 0.905 |
| 3000 | 0.97 | 0.9 |
| 3500 | 0.965 | 0.895 |
| 4000 | 0.96 | 0.905 |
| 4500 | 0.968 | 0.905 |
| 5000 | 0.97 | 0.875 |
| 5500 | 0.965 | 0.85 |
| 6000 | 0.965 | 0.8 |

**Table 4**: The real to stoichiometric fuel ratios associated with different RPMs.

Combustion is modeled using quasi dimensional models. In this regard, a two zone model is adopted and analyzed in our computer code. The heat release is evaluated using the same code considering a two zone Wiebe model (Ferguson and Kirkpatrick 2000).

The delay in the combustion initiation is predicted based on Benson-Whitehouse model (Ramos 1992). Heat transfer of the combustion chamber is investigated based on the modified Woschni's model (Ferguson and Kirkpatrick 2000). The governing equations of the mean temperature, the mean convection heat transfer coefficient, and the rates of pressure and energy release per crank angle may be found using the first law of thermodynamics. The employed geometric parameters are shown in Fig. 1.

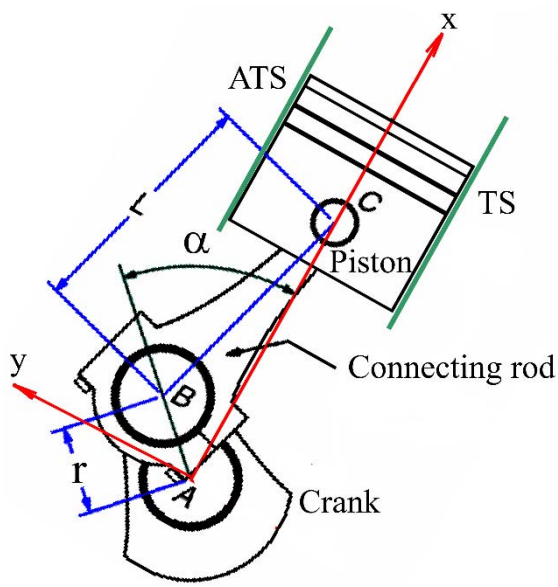


**Figure 1**: Geometric parameters of the crank-piston mechanism.

It can be shown that variations of the pressure in the combustion chamber can be determined based on the following differential equation (Abu-Nada et al. 2008):

$$\frac{dP}{d\alpha}=\frac{\gamma-1}{V}Q_{in}\frac{dx_b}{d\alpha}-\frac{dQ_w}{d\alpha}-\gamma\frac{P}{V}\frac{dV}{d\alpha} \tag{3}$$

where:

$$\frac{dQ_w}{d\alpha}=h_g(\alpha)\left\{\pi b\left[r+l-\sqrt{l^2-r^2\sin^2\alpha}-r\cos\alpha\right]+\pi/2b^2\right\}(T_g(\alpha)-T_w)/N \tag{4}$$

$$\frac{dV}{d\alpha}=\frac{\pi b^2 S}{8}\left[1+(r^2-\sin^2\alpha)^{\frac{-1}{2}}\cos\alpha\right]\sin\alpha \tag{5}$$

where, $S$, $b$, $V$, $N$, and $\gamma$ are the stroke, piston diameter, cylinder volume, engine RPM, and ratio of the constant pressure to constant volume values of the specific heat, respectively. $P$, $x_b$, $Q_{in}$,

$Q_w$, $h_g$, $T_g$, and $T_w$ are respectively, the instantaneous pressure, Wiebe function, total amount of heat input due to combustion of the fuel in one cycle *f*, the heat energy transferred to the ambient through the cylinder wall, Woschni's convective heat transfer coefficient (Woschni 1967; Karamangil et al. 2006), temperature of the combustion products, and temperature of the cylinder wall. Subscripts $w$ and $g$ stand for the cylinder wall and gasses, respectively. The derivation procedure (performed by the authors) is not included here due to space restrictions. The resulted partial differential equations are solved by the Runge-Kutta numerical time integration method.

These data are employed to perform the required heat transfer analyses. The theoretically determined temperature distributions are validated by the experimental results measured by the high temperature plugs (templugs).

## 3 DYNAMIC FORCES, THERMAL, AND THERMOELASTIC STRESS ANALYSES

In the present research, the forces are determined based on the written Matlab code according to a textbook by Erdman et al. (2001), and the ABAQUS CAE software, through exactly modeling the contact and large displacements non-linearities. Denoting the distance between center of gravity of the connecting rod to center of the gudgeon pin by $b$ and angle between the connecting rod and the sliding direction by $\beta$, one may write the acceleration of the center of gravity of the connecting rod as (Erdman et al. 2001):

$$\mathbf{a}_G^p = \left[ b\ddot{\beta}\sin(\beta) + b\dot{\beta}^2\cos(\beta) + a_{piston} \right]\mathbf{i} + \left[ b\ddot{\beta}\cos(\beta) - b\dot{\beta}^2\sin(\beta) \right]\mathbf{j} \tag{6}$$

where $\mathbf{i}$ and $\mathbf{j}$ are respectively, the base vectors in the $x$ and $y$ directions of Fig. 1. Therefore, denoting the inertial forces transferred between the piston and the connecting rod and between the connecting rod and the crank shaft by $F_1$ and $F_2$ respectively, one may write the following equation based on Newton's second law:

$$\begin{aligned}
F_{1a} &= F_g\cos\beta - \frac{I_G\ddot{\beta} - F_g l\sin\beta - (l-b)m_c\left(a_{Gx}\sin\beta + a_{Gy}\cos\beta\right)}{(l-b)\cos\beta + b\cos\beta}\sin\beta \\
F_{1n} &= F_g\sin\beta + \frac{I_G\ddot{\beta} - F_g l\sin\beta - (l-b)m_c\left(a_{Gx}\sin\beta + a_{Gy}\cos\beta\right)}{(l-b)cos\beta + b\,cos\beta}\cos\beta \\
F_{2a} &= \left(F_g + m_c a_{Gx}\right)\cos\beta - \frac{I_G\ddot{\beta} - F_g l\sin\beta - bm_c\left(a_{Gx}\sin\beta + a_{Gy}\cos\beta\right)}{(l-b)cos\beta + b\,cos\beta}\sin\beta \\
F_{2n} &= F_g\sin\beta + \frac{I_G\ddot{\beta} - F_g l\sin\beta - bm_c\left(a_{Gx}\sin\beta + a_{Gy}\cos\beta\right)}{(l-b)cos\beta + b\,cos\beta}\cos\beta
\end{aligned} \tag{7}$$

where the subscripts $a$ and $n$ denote directions along and normal to the connecting rod, respectively and $F_g$ and $I_G$ are respectively, the combustion gas force and moment of inertia of the connecting rod around its center of gravity.

The frictional forces including the mixed and hydrodynamic ones and the distributed inertia forces are taken into account. Following detailed studies by Thring (1992) and Dowson et al. (1996), the mean effective friction traction may be determined from:

$$f_{mep} = 6.89\frac{P_i}{P_a}\left[0.088r_c + 0.182r_c\left(1.33 - 2.38\times10^{-2}S_p\right)\right] \tag{8}$$

where $P_i$, $P_a$, $r_c$, and $S_p$ are the intake pressure, atmospheric pressure, compression ratio of the engine, and the mean speed of the piston, respectively. In the considered engine, SAE10w-40 lubricant oil whose dynamic viscosity varies with temperature as follows, is used:

$$\eta(T) = 1.14e^{-10}\exp\left(\frac{1033.34}{T + 120.8}\right) \tag{9}$$

Based on the convection heat transfer between the piston's top surface and the combustion mixture, heat transfer between the rings and the skirt and the cylinder and consequently, the coolant water, the heat transfer between the gudgeon pin and the coolant oil film, the thermal loads of the piston are determined. Finally, a thermoelastic stress analysis is performed. Details of the type of the employed constitutive model and the temperature-dependent material properties are mentioned in the results section.

## 4 THE FATIGUE LIFE ASSESSMENT ALGORITHM

As may be expected, the resulting thermoelastic stress components vary in a non-proportional manner. Furthermore, they fluctuate with non-zero mean stresses. A number of evaluations available in the literature (Socie, 1987; Li et al., 2011; Papuga, 2011; Fatemi and Shamsaei, 2011; Castro et al., 2014) demonstrate that satisfactory correlations can be obtained using the critical plane approach, both in the low and high cycle fatigue regimes. These satisfactory correlations were observed for a number of engineering materials, notch geometries, and loading conditions (including non-proportional histories with or without superimposed mean stresses).

Based on some observations (Papuga, 2011; Castro et al., 2014) and the comprehensive discussions already published by Shariyat (2008; 2009a,b; 2010), the accuracy of the traditional fatigue life assessment criteria as well as the available critical plane high cycle fatigue (HCF) criteria depends on a number of factors, e.g., accuracy of the material constants, experience of the user in modeling the loading events, and accuracy of the computed stresses and strains used as input in the fatigue criterion. Although the traditional von Mises criterion that is the base for many well-known fatigue analysis softwares, such as MSC Fatigue and FEMFAT, may lead to erroneous results in the mentioned circumstances, its results may be enhanced by employing Sine's idea of the mean stress (Socie and Marquis 2000; Schijve 2009) and incorporating the mean stress effect, using Goodman, Gerber, or Soderberg fatigue failure relations:

$$\text{Goodman's linear relation: } \frac{\sigma_a}{\sigma_N} + \frac{\sigma_m}{\sigma_u} = 1 \tag{10}$$

$$\text{Gerber's parabolic relation: } \frac{\sigma_a}{\sigma_N}+\left(\frac{\sigma_m}{\sigma_u}\right)^2=1 \tag{11}$$

$$\text{Soderberg's linear relation: } \frac{\sigma_a}{\sigma_N}+\frac{\sigma_m}{\sigma_y}=1 \tag{12}$$

where $\sigma_a$, $\sigma_m$, $\sigma_N$, $\sigma_y$, and $\sigma_u$ are the amplitude, mean stress, equivalent reversible (fatigue strength), yield, and ultimate stresses, respectively.

Among the critical plane high cycle fatigue (HCF) criteria, Findley's criterion has been proven to be the most accurate one (Bernasconi et al. 2008). Findley's criterion may be expressed as (Findley 1959):

$$(\tau_a+k\sigma_n)_{\max(\theta,\psi,\varphi)}=f \tag{13}$$

where:

$$k=\frac{2-\sigma_{R=-1}/\tau_{R=-1}}{2\sqrt{\sigma_{R=-1}/\tau_{R=-1}-1}},\quad f=\sqrt{\frac{(\sigma_{R=-1})^2}{4(\sigma_{R=-1}/\tau_{R=-1}-1)}} \tag{14}$$

According to this criterion, the critical plane is a plane where $\max_{\theta,\varphi,\psi,t}(\tau_a+k\sigma_n)$ occurs. $\theta,\varphi$, and $\psi$ are the Eulerian angles (Fig. 2) and $t$ denotes the time. $\tau_a$ and $\sigma_n$ are the shear stress amplitude and the normal stress component, respectively. Denoting the fatigue strength amplitudes corresponding to the specified $\left(R=\sigma_{\min}/\sigma_{\max}\right)$ and $\left(R=\tau_{\min}/\tau_{\max}\right)$ ratios, respectively, by $\sigma_R$ and $\tau_R$, Shariyat (2009a) has proposed a modified Findley's criterion as:

$$\tau_{eq}=\max_{\theta,\varphi,\psi,t}(\tau_a+k\sigma_n)/\left(\sqrt{1+k^2}\,\tau_{R=-1}/\tau_R\right) \tag{15}$$

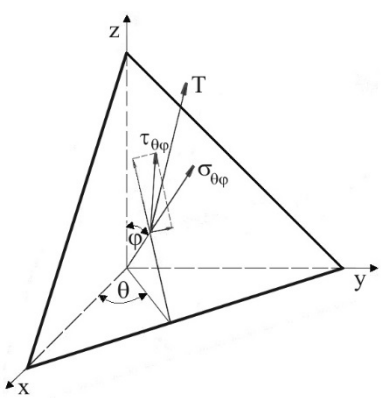


**Figure 2**: Resultant shear and normal stresses acting on a representative material plane.

Based on Goodman and Gerber mean stress correction factors, $\sigma_R$ may be expressed as:

Modified Goodman's line equation:

$$\sigma_R = \begin{cases} \sigma_{R=-1}\left(1-\dfrac{\sigma_m}{\sigma_u}\right) & 0 \le \sigma_m \\ \sigma_{R=-1} & \sigma_m \le 0 \end{cases} \tag{16}$$

Gerber's equation:

$$\sigma_R = \sigma_{R=-1}\left[1-\left(\frac{\sigma_m}{\sigma_u}\right)^2\right] \tag{17}$$

Similar equations may be written for $\tau_R$. Since the minus and plus mean stresses appear with similar effects in Gerber's equation, Goodman's equation is used in the present research to account for the mean stress effect.

It is known that Liu-Zener criterion is the most accurate criterion among all the available high cycle fatigue criteria. Recently, Shariyat (2009b) has modified this criterion and through verifying results of the criterion by many experimental results (including one-, two-, and three-dimensional load conditions), proved that the proposed criterion leads to more accurate results. However, the criterion has not been examined for situations where thermoelastic stresses are induced. In the present work results of the mentioned criterion are examined for the thermoelastic stress fields. In contrast to the available HCF criteria, Shariyat's criterion has been proposed based on tracing the microscopic instantaneous fatigue failures and is suitable for non-proportional three-dimensional stress fields with stress components that vary with random frequencies and random amplitudes. This integral-type criterion has the following form:

$$\sqrt{\frac{15}{8\pi}\int_0^{2\pi}\int_0^{\pi}(\hat{\alpha}\tau_{\theta\varphi}^2+\hat{\beta}\sigma_{\theta\varphi}^2)\sin\varphi\, d\varphi\, d\theta} + \hat{\delta}\sigma^H = \sigma_{eq} \tag{18}$$

where the normal and resultant shear components acting on the material sections are (Shariyat, 2009b):

$$\tau_{\theta\varphi} = \left\{\left[\sin\varphi\left(\frac{\sigma_x-\sigma_y}{2}\sin 2\theta-\tau_{xy}\cos 2\theta\right)+\cos\varphi(\tau_{xz}\sin\theta-\tau_{yz}\cos\theta)\right]^2 + \left[\sin\varphi\cos\varphi\left(\frac{\sigma_x+\sigma_y}{2}+\frac{\sigma_x-\sigma_y}{2}\cos 2\theta+\tau_{xy}\sin 2\theta-\sigma_z\right)+\cos 2\varphi\left(\tau_{xz}\cos\theta+\tau_{yz}\sin\theta\right)\right]^2\right\}^{1/2} \tag{19}$$

$$\sigma_{\theta\varphi} = \sin^2\varphi\left(\frac{\sigma_x+\sigma_y}{2}+\frac{\sigma_x-\sigma_y}{2}\cos 2\theta+\tau_{xy}\sin 2\theta\right)+\sin 2\varphi\left(\tau_{xz}\cos\theta+\tau_{yz}\sin\theta\right)+\sigma_z\cos^2\varphi$$

and $\sigma^H$ is the spherical stress component and:

$$\hat{\alpha} = \frac{1}{45\left(1-3\tilde{\eta}\right)^2}(189\tilde{\xi}^2+108\tilde{\eta}-9\tilde{\xi}^2\tilde{\zeta}^2+12\tilde{\eta}^{-1}+21\tilde{\zeta}^2-81\tilde{\eta}^2-126\tilde{\xi}\tilde{\zeta}-\tilde{\eta}^{-2}-54)\,, \tag{20}$$

$$\hat{\beta}=\frac{-1}{30\left(1-3\tilde{\eta}\right)^{2}}\left(6+3\tilde{\xi}\tilde{\zeta}-\tilde{\eta}^{-1}-9\tilde{\eta}\right)^{2},\ \hat{\delta}=\frac{1}{2\left(1-3\tilde{\eta}\right)}\left(3\tilde{\xi}\tilde{\zeta}-9\tilde{\eta}+\tilde{\eta}^{-1}\right),$$

$$\tilde{\zeta}=\frac{\sigma_{R=-1}\left(1-\sigma_m/\sigma_u\right)}{\tau_{R=-1}\left(1-\tau_m/\tau_u\right)},\ \tilde{\eta}=\frac{\sigma^{H}_{R=-1}\left(1-\sigma^{H}_m/\sigma^{H}_u\right)}{\sigma_{R=-1}\left(1-\sigma_m/\sigma_u\right)},\ \tilde{\xi}=\frac{\sigma^{H}_{R=-1}\left(1-\sigma^{H}_m/\sigma^{H}_u\right)}{\tau_{R=-1}\left(1-\tau_m/\tau_u\right)}$$

The related fatigue life assessment flow chart is illustrated in Fig. 3.

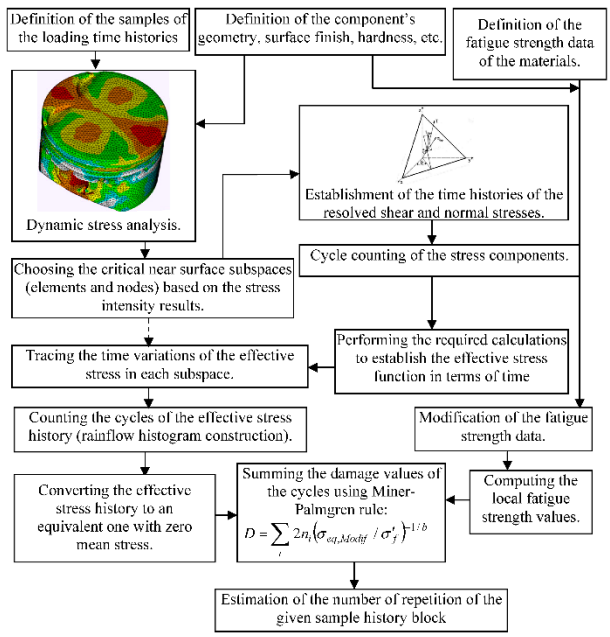


**Figure 3**: Flow chart of the employed fatigue life assessment algorithm.

## 5 RESULTS

Properties of the gasoline vary with temperature. Since temperature of the fuel varies during the 720 degrees rotation of the crank (one combustion cycle), the following equation is used to predict the properties values at any specified temperature:

$$\overline{C}_{p\ fuel}=A_{f1}+A_{f2}.T+A_{f3}.T^{2}+A_{f4}.T^{3}+A_{f5}/T^{2} \tag{21}$$

The coefficients $A_{f1}$ to $A_{f5}$ are given in Table 5.

| Fuel | $A_{fs}$ | $A_{f1}$ | $A_{f2}$ | $A_{f3}$ | $A_{f4}$ | $A_{f5}$ |
|---|---|---|---|---|---|---|
| $C_{8.26}\ H_{15.5}$ | 14.64 | -24.078 | 256.63 | -201.68 | 64.75 | 0.5808 |
| $C_{7.26}\ H_{13.1}$ | 14.37 | -22.501 | 277.99 | -177.26 | 56.048 | 0.4845 |

**Table 5**: Coefficients of the temperature-dependency of the material properties of the fuel (Heywood, 1988).

While properties of the air may be determined based on the available references, variations of the combustion products may be determined based on the following equation ($\theta = T/100$) (Borgnakke and Sonntag 2009):

$$\begin{cases} \bar{C}_{p\,N_2} = 39.06 - 512.79\theta^{-1.5} + 1072.72\theta^{-2} - 820.4\theta^{-3} \\ \bar{C}_{p\,H_{2O}} = -37.57 + 30.529\theta^{0.5} - 4.1034\theta \mp .024198\theta^{2} \\ \bar{C}_{p\,CO_2} = 143.05 - 183.54\theta^{0.25} + 82.751\theta^{0.5} - 3.6989\theta \\ \bar{C}_{p\,O_2} = 37.432 + .020102\theta^{0.1.5} - 178.57\theta^{-1.5} + 236.88\theta^{-2} \end{cases} \tag{22}$$

Property of the exhaust gases may be determined from (Borgnakke and Sonntag 2009):

$$\bar{C}_{p\,Pollutant} = \frac{\bar{C}_{p\,N_2} + \bar{C}_{p\,H_2O} + \bar{C}_{p\,CO_2} + \bar{C}_{p\,O_2}}{8.26 + 15.5/2 + 45.6276} \tag{23}$$

Fig. 4 compares the pressure of the combustion mixture versus the crank angle curves predicted by the theoretical results (results of our computer code) with those measured experimentally for the gasoline and CNG fuels, for the 6000 RPM situation (corresponds to the maximum power), as a typical case. The theoretical results are in a good agreement with the experimental results. Furthermore, results of Figs. 4 reveal that replacing the gasoline with the natural gas may lead to significant changes in the resulting pressure profile in 6000 RPM.

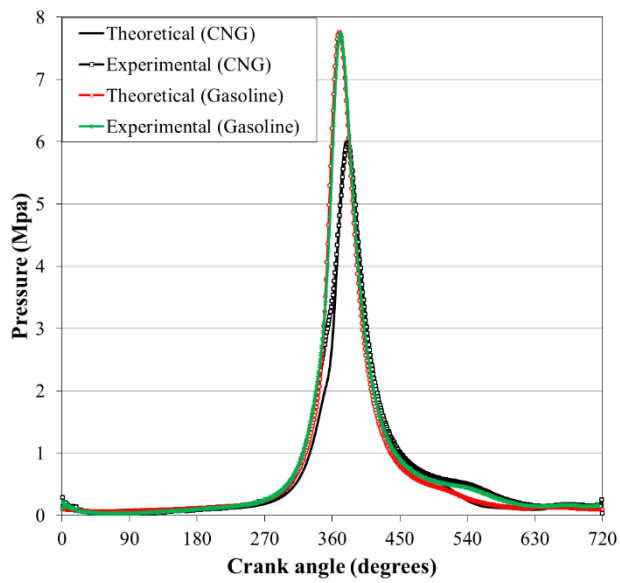


**Figure 4**: In-cylinder pressure variations versus crank angle for a set of theoretical and experimental results using gasoline and natural gas, at 6000 RPM.

Figures 5 and 6 illustrate variations of the computed temperature of the combustion mixture and the coefficient of the heat convection of the top surface of the piston, with the crank angle at

6000 RPM, respectively. Since the temperature distributions are somewhat identical, due to higher coefficient of the convection heat transfer, it seems that the thermal losses may be higher for the CNG engine. Figs. 7 and 8 illustrate the vertical and horizontal components of the resultant forces exerted on the piston, respectively for the gasoline and CNG engines at 3500 (corresponding to the maximum torque) and 6000 RPMs. As may be noted from Figs. 7 and 8, the maximum forces are exerted slightly after the combustion initiation. Furthermore, the vertical component is the dominant one.

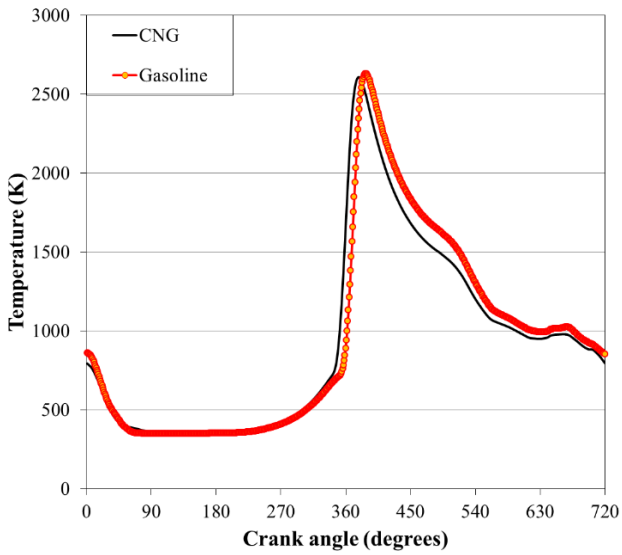


**Figure 5**: Comparison of the mixture temperature for the gasoline and CNG engines at 6000 RPM.

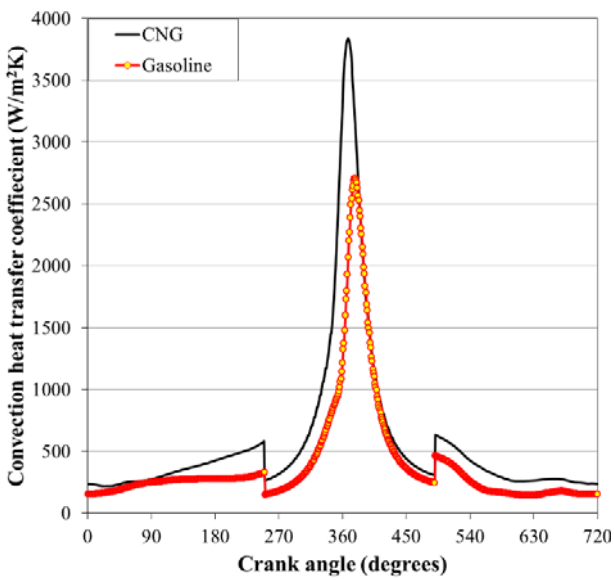


**Figure 6**: Comparison of the coefficients of the convection heat transfer for the gasoline and CNG engines at 6000 RPM.

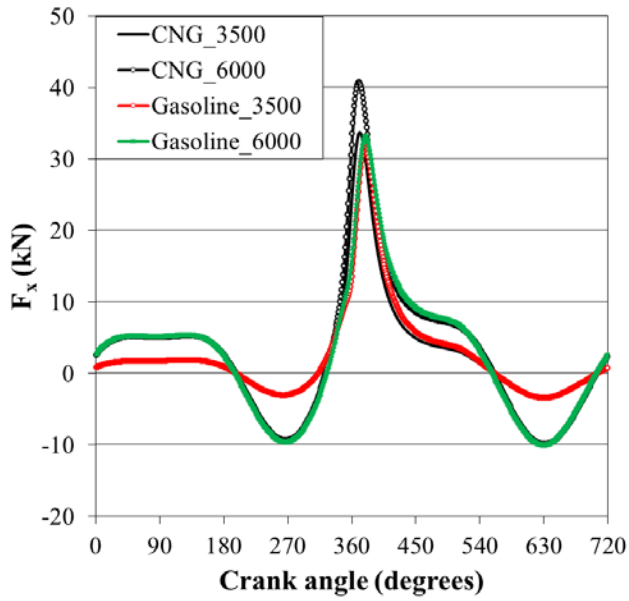


**Figure 7**: A comparison among the vertical components of the resultant forces acting on the piston at 3500 and 6000 RPMs, for the gasoline and CNG engines.

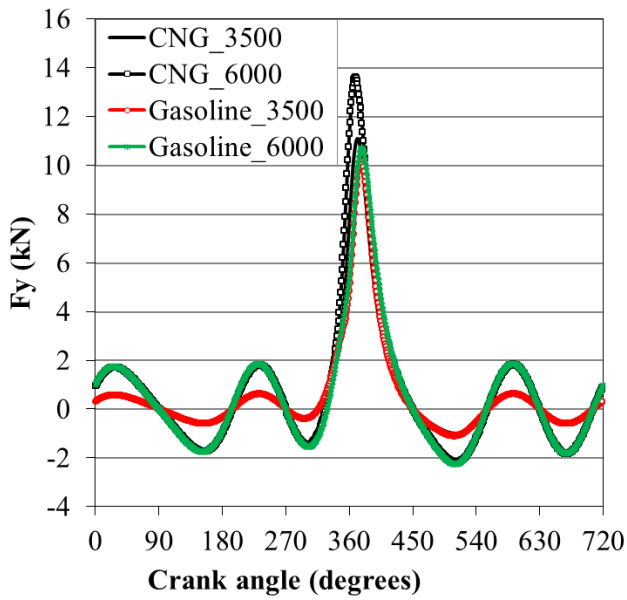


**Figure 8**: A comparison among the horizontal components of the resultant forces acting on the piston at 3500 and 6000 RPMs, for the gasoline and CNG engines.

Time variations of the frictional force are shown in Fig. 9 for the thrust side of the piston's skirt, at 3500 and 6000 RPMs for the gasoline and CNG fuels. As may be readily seen, the frictional forces at the top dead centre (TDC) and bottom dead center (BDC) are of boundary nature (Tung

and McMillan 2004) and consequently, high whereas at the midway point, the friction is of a hydrodynamic nature and leads to small frictional forces.

Figure 10 illustrates the force components exerted by the gudgeon pin on the piston and vice versa based on our results and results of the AVL-GLIDE software.

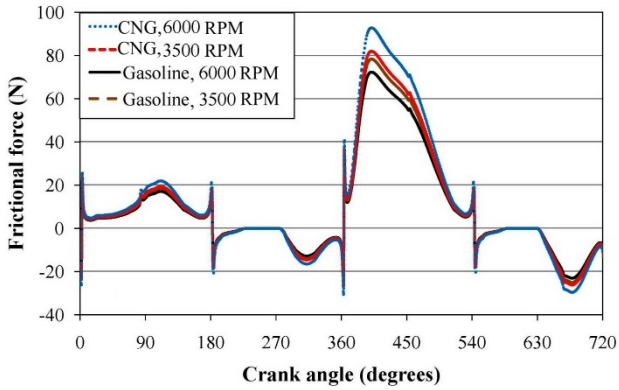


**Figure 9**: Variations of the frictional forces for the thrust side of the piston's skirt at 3500 and 6000 RPMs for gasoline and CNG engines.

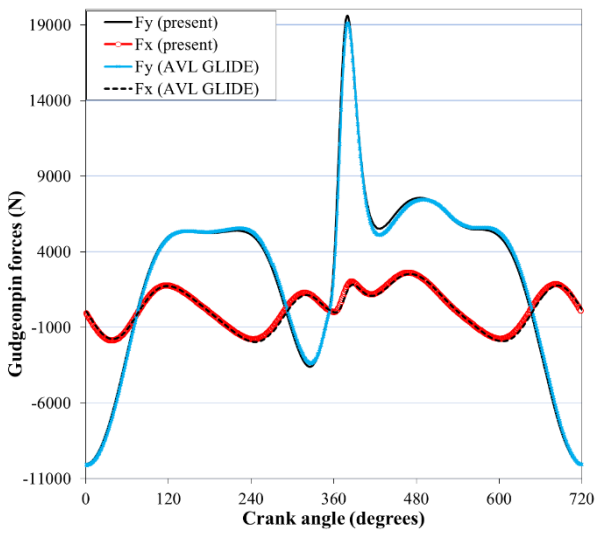


**Figure 10**: A comparison between present and AVL-Glide software predictions for force components exerted by the gudgeon pin on the piston (CNG engine at 6000RPM).

The finite element analysis (FEA) model of the piston has been constructed in Hypermesh software. Optimized second-order Lagrangian elements are adopted to avoid abrupt jumps in the stress components at the mutual boundaries of the elements. The FEA model is validated through a modal analysis in the NASTRAN/PATRAN software. After accurately defining of the contact regions and constraints, the inertial, frictional, and the thermomechanical combustion loads obtained in the foregoing steps are imposed. In the contact region of the rings, skirt, and pin of the piston, the

mean temperature of the lubricant film and the proper coefficients of the convection heat transfer are used.

Figure 11 illustrates the temperature rise distributions of the piston in the 6000 RPM for both gasoline and CNG engines, as typical results. The temperature rise distributions have been validated experimentally by means of the TEMPLUGs shown in Fig. 12. Comparison of the experimental and theoretical results reported in Table 6 for the gasoline fuel, generally verifies the present analytical approach.

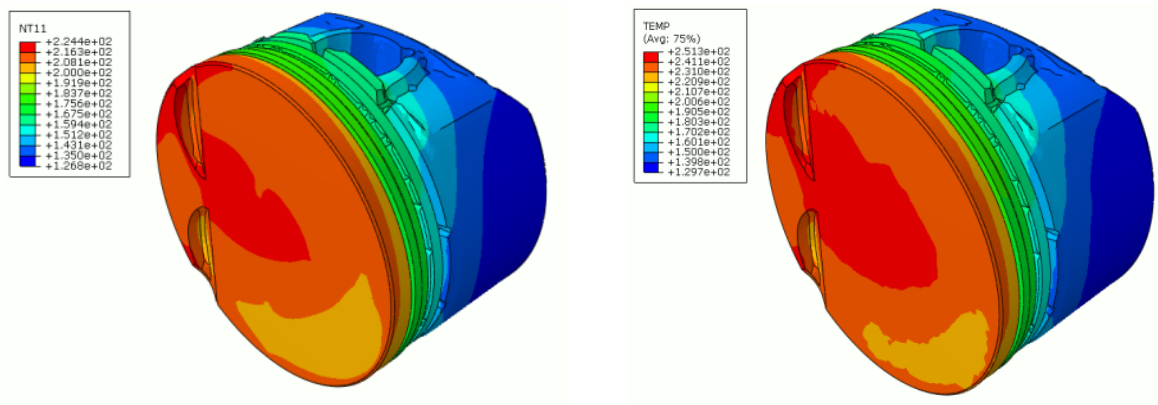


(a) (b)

**Figure 11**: Temperature rise (°C) distributions in 6000 RPM for the (a) gasoline, and (b) CNG engines.

| Templug location | Experimental results | Theoretical results |
|---|---|---|
| 1 | 222 | 220 |
| 2 | 235 | 229 |
| 3 | 207 | 205 |
| 4 | 228 | 225 |
| 5 | 244 | 242 |
| 6 | 249 | 245 |
| 7 | 238 | 235 |
| 8 | 230 | 226 |
| 9 | 237 | 247 |
| 10 | 226 | 220 |
| 11 | 230 | 225 |

**Table 6**: Comparison of the experimental and theoretical temperature rise (°C) results, for various points of the piston, in the 6000 RPM for the gasoline engine.

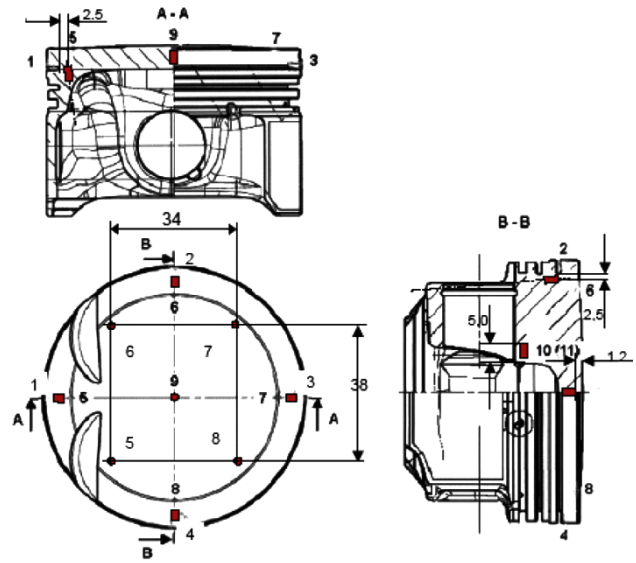


(a)

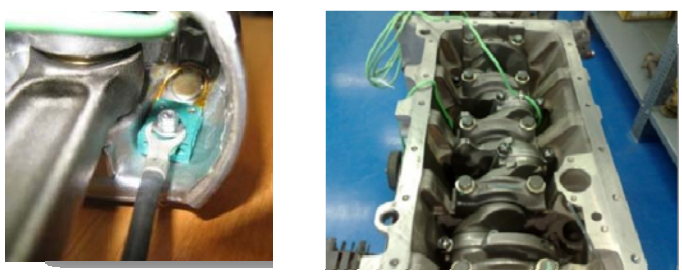

(b)

**Figure 12**: The temperature plugs used to validate the computed temperatures: (a) locations and (b) installation.

The thermal stresses stem mainly from the non-uniform temperature distribution. The thermoelastic and subsequently, the fatigue analysis now can be accomplished based on the obtained time histories of the temperature distributions and the mechanical loads. Since these analyses are structural ones, the mechanical material properties have to be known as well. The piston is fabricated from the cast AlSi12Cu1Mg1Ni1 low Si alloy, i.e. the M124 alloy. The piston was subjected to T5 (cooling from hot working and artificially aging at temperatures above ambient) and T7 (solution heat-treatment followed by artificially over-aging) heat treatments. Some of the material properties have been provided by the supplier (such as the material properties and the monotonic static properties). Although the fatigue strengths have been given by the piston supplier, some fatigue experiments are carried out by the authors to ensure that this information is accurate enough. The relevant test procedures may be found e.g., in papers by Lipski and Mroziński (2012) and Konecna et al. (2015). The mechanical and thermal properties of the piston are really temperature-dependent ones and their temperature-dependency has to be considered to present a relatively accurate analysis. The mechanical and thermal material properties of the employed M124 alloy are summarized in Table 7. Information reported in Table 7 is in a close concordance with the data reported by

MAHLE GmbH (2012) for the general M124 piston alloy. A typical trend of variations of the coefficients of the convection heat transfer was shown in Fig. 6, for the gasoline and CNG engines.

| Material property | Temperature (°C) | Value |
|---|---|---|
| Young's Modulus (GPa) | 20 | 79 |
| | 150 | 76 |
| | 250 | 72 |
| | 350 | 64 |
| Thermal conductivity (W/mK) | 20 | 141 |
| | 350 | 152 |
| Poisson ratio | - | 0.33 |
| Density (kg/m$^3$) | 20 | 2680 |
| Thermal expansion ($10^{-6}$m/mK) | 20-100 | 19.6 |
| | 20-200 | 20.6 |
| | 20-300 | 21.4 |
| | 20-400 | 22.1 |
| Specific heat (kj/kgK) | - | 864 |
| Tensile strength (MPa) | -200 | 328 |
| | -100 | 296 |
| | 20 | 241 |
| | 150 | 207 |
| | 250 | 117 |
| | 350 | 53 |
| Melting point (°C) | - | 571 |
| Fatigue strength (MPa) | 20 | 108 |
| | 150 | 84 |
| | 250 | 53 |
| | 350 | 26 |

**Table 7**: Temperature-dependent mechanical and thermal material properties of the pistons fabricated from M124 alloy with T5 and T7 heat treatments, as well as the monotonic (static) and fatigue strengths.

Since the material properties reported in Table 7 cover a wide range of the temperatures, they may be used for thermoelastic and fatigue analyses of all points of the piston. The material properties may be interpolated for temperatures that are not appeared in Table 7. However, the most critical region has a specific temperature that fluctuates slightly with time.

The heat transfer sources are the temperature rise of the fuel mixture, e.g., that shown in Fig. 5, the lubrication jet injected under the piston, the lubrication layers and the cooling water at the

ring and skirt regions. The heat transfer coefficients are calibrated further based on the experimental information gathered from the Templug sensors.

The relevant mechanical von Mises stresses are shown in Fig. 13, for the most critical situation (370 degrees of the crank angle) at 6000 RPM for the CNG engine, as representative results. The maximum calculated temperature is 252 (°C) which shows a good agreement with the result measured by the templugs (249 °C).

Regions with greatest von Mises equivalent stresses may not be generally considered as regions with worst fatigue lives. Fig. 14 shows the most critical element in the thermomechanical loading. This element is detected by fatigue results obtained by the MSC Fatigue software (as explained later) and present results. Time variations of the von Mises equivalent mechanical stress of the critical region are depicted in Fig. 15 for a complete combustion cycle of the gasoline as well as CNG engines, for 3500 and 6000 RPMs. From these figures, it may be deduced that the maximum and minimum stresses occur at crank angles of 370 and 1 degrees, respectively.

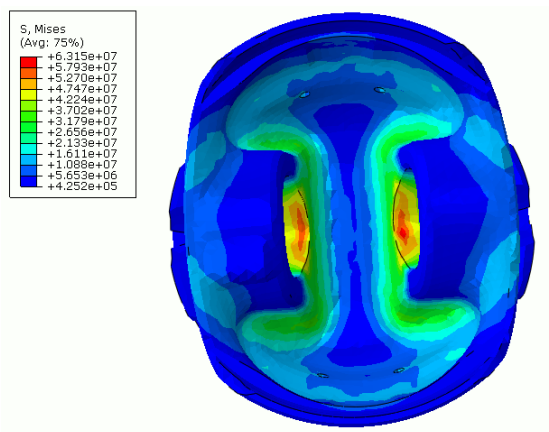


**Figure 13**: The resulting mechanical von Mises stresses at 6000 RPM, for the CNG engine.

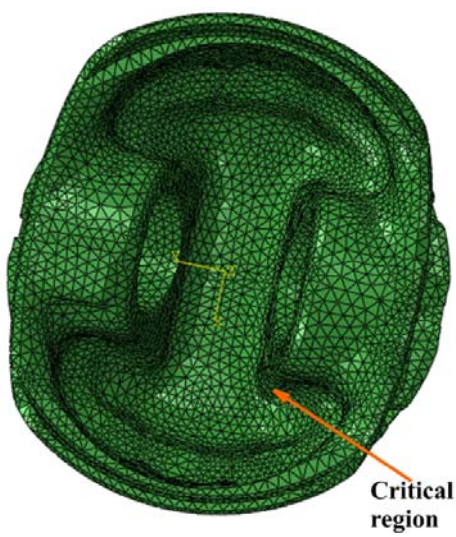


**Figure 14**: Orientations of the most critical region.

As has been mentioned in Sec. 4, in the present research, the fatigue life results are extracted based on the modified von Mises, modified version of Findley and Liu-Zener theories proposed by Shariyat, and the experimental methods. The employed fatigue life assessment algorithm has not been proposed by any other authors before. The equivalent Findley stresses (Eq. 11) are computed at the critical points of the piston and the relevant fatigue lives have been calculated based on computer codes written by the authors, for the 720 degrees rotation of the crank. Some fatigue damages predicted by different approaches, various engine RPMs and fuel types are shown in Table 8 for the critical region, as typical results.

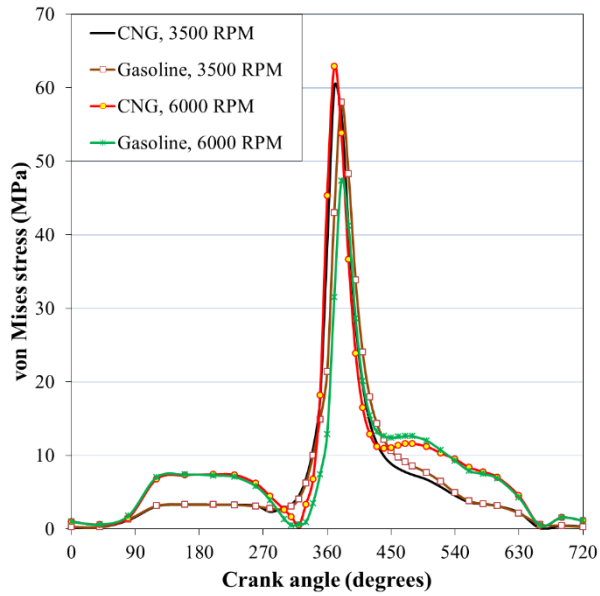


**Figure 15**: Variations of the von Mises stress of the critical node for the complete combustion cycle of the gasoline as well as CNG engines, at 3500 and 6000 RPMs.

| Fatigue life assessment approach | Gasoline (3500RPM) | CNG (3500 RPM) | Gasoline (6000RPM) | CNG (6000RPM) |
|---|---|---|---|---|
| von Mises (Goodman mean stress correction) | 2.1316e-10 | 5.8102e-10 | 1.6211e-11 | 3.5025e-9 |
| von Mises (Gerber mean stress correction) | 6.3924e-11 | 1.6768e-10 | 5.6012e-12 | 1.9938e-9 |
| von Mises (Soderberg mean stress correction) | 7.2651e-10 | 2.1891e-9 | 4.1897e-11 | 9.3645e-9 |
| Modified Findley | 17.4480e-12 | 7.9051e-12 | 9.0612e-13 | 8.1219e-11 |
| Shariyat's criterion | 5.6381e-12 | 6.6004e-11 | 6.9281e-13 | 1.9069e-10 |
| FEMFAT software | 6.9e-12 | 7.22e-11 | 9.31e-13 | 1.1e-10 |

**Table 8**: Fatigue damages predicted by different approaches for the critical region, for various RPMs.

As a second stage, two standard histograms are adopted to simulate the service thermomechanical loads and extract the fatigue results. The corresponding block programs are described in Tables 9 and 10. The first standard block program corresponds to the so-called 800hr durability test under

mechanical loads whereas the second one is associated with the so-called 400 hr durability test under thermal loads. The corresponding fatigue test conditions are also specified in the mentioned tables. These tests have been adopted based on a compromise between Peugeot and FEV automotive companies durability test procedures.

As mentioned before, the most critical regions of the piston are the pin hole, piston's crown, and piston's skirt (at the thrust side) (precisely, the region indicated in Fig. 14). The fatigue damage contours obtained by FEMFAT and FESAFE softwares (Fig. 16), confirm this conclusion.

| Event order | Duration [minutes] | Engine speed [RPM] | Load specifications |
|---|---|---|---|
| 1 | 5 | 6000 | rated power |
| 2 | 4 | 2000 | BMEP= 2 bar |
| 3 | 5 | 3500 | max torque |
| 4 | 1 | 750 | low idle |

**Table 9**: Block program of the 800 hr mechanical engine durability test [outlet coolant water temperature= $90^{+3}$ (°C) and Max. oil temperature= 140 (°C)].

| Event order | Duration [minutes] | Engine speed [RPM] | Load specifications | Outlet coolant water temperature [°C] |
|---|---|---|---|---|
| 1 | 9.5 | 6000 | rated power | $90^{+3}$ |
| 2 | 4.5 | 750 | low idle | $30^{+10}$ |

**Table 10**: Block program of the 400 hr thermal engine durability test.

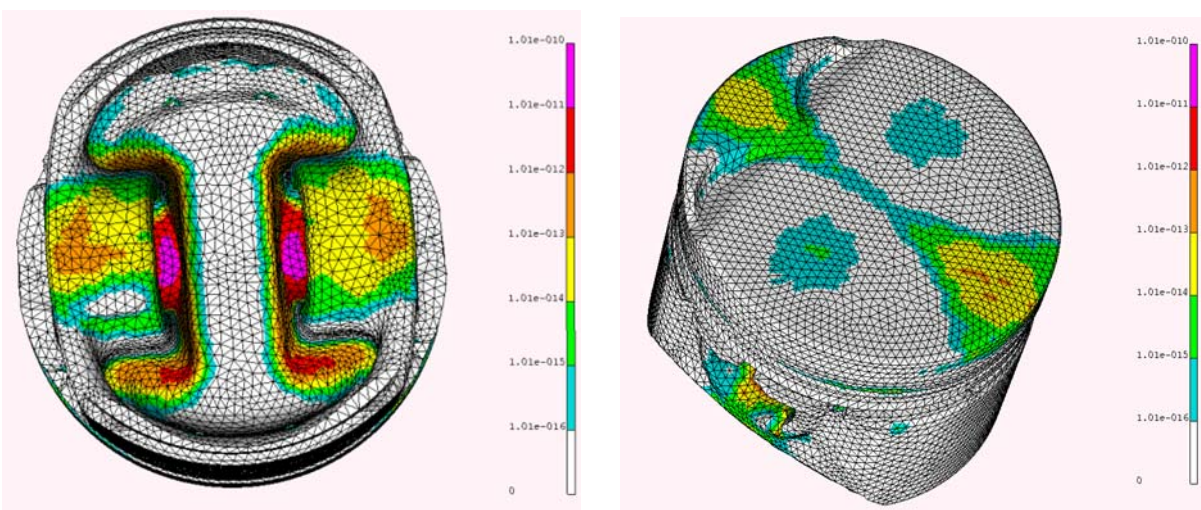


**Figure 16**: Fatigue damage contours of the piston derived by the FEMFAT software, for the CNG engine (at 6000 RPM).

Figure 17 illustrates the experimental fatigue lives according to the observed fatigue failures, the number of repetitions of fatigue tests carried out under identical conditions, the scatter of the ex-

perimental data, and the fatigue lives predicted by various fatigue theories for the 800 hr durability tests of both the gasoline and CNG engines. Fatigue failures have been detected based on visual NDT techniques, e.g. spot check for micro-crack detection. Some of the defects occurred for the piston through the fatigue tests are shown in Fig. 18. It is known that in non-proportional loadings, von Mises criterion usually leads to results that are extremely conservative (Socie and Marquis 2000). In the present analysis, von Mises criterion is modified using Goodman, Gerber, and Soderberg mean stress corrections (Eqs. 10-12). Although modified von Mises criterion has been employed in the present research, the relevant results show significant errors. Fig. 17 reveals that employing Gerber and Soderberg mean stress corrections leads to most and least accurate results for the von Mises-type criteria. Furthermore, Fig. 17 reveals that modified Findley and Shariyat's criteria lead to more accurate results with the modified Shariyat's criterion regenerates the experimental results more accurately. Moreover, the relative discrepancies between the theoretical results are different, to some extent, for the gasoline and CNG engines. Results of various theories are compared in Fig. 19 with the experimental results of the 400hr durability test. As before, it was intended to use at least four fatigue failure test results to present a stronger discussion. As it may be readily seen, results of Shariyat's criterion are closer to the experimental results. Results presented in Figs. 17 and 19 reveal that in contrast to other criteria, the modified Findley criterion has slightly underestimated the fatigue lives, especially for the CNG engine.

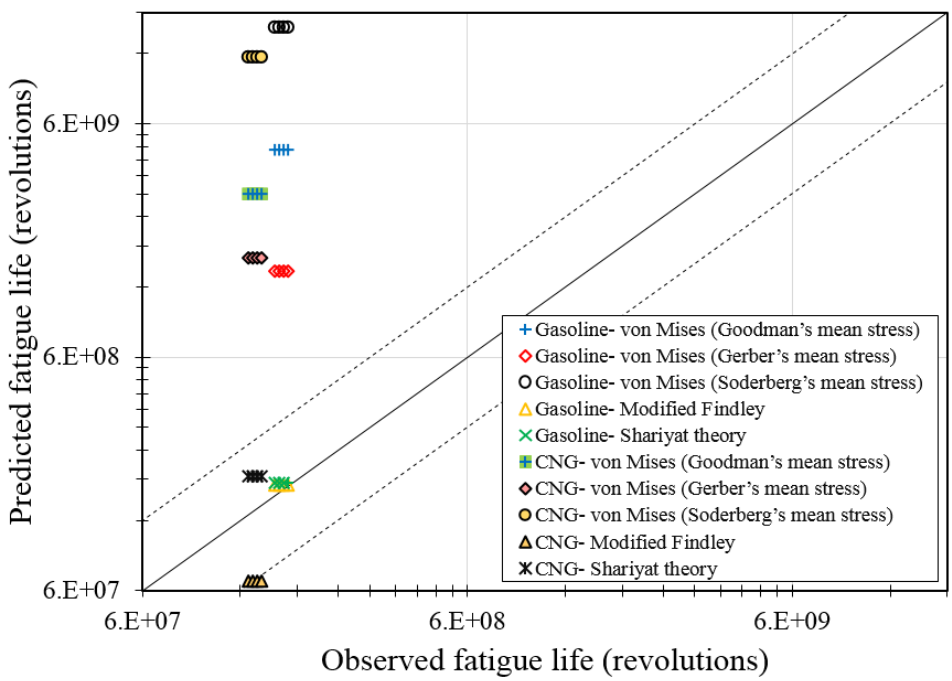


**Figure 17**: Comparison of the observed (experimental) and estimated fatigue lives based on various theories, for the so-called 800 hr durability tests of both the gasoline and CNG engines.


**Figure 18**: Some of the observed piston's defects during the fatigue tests.

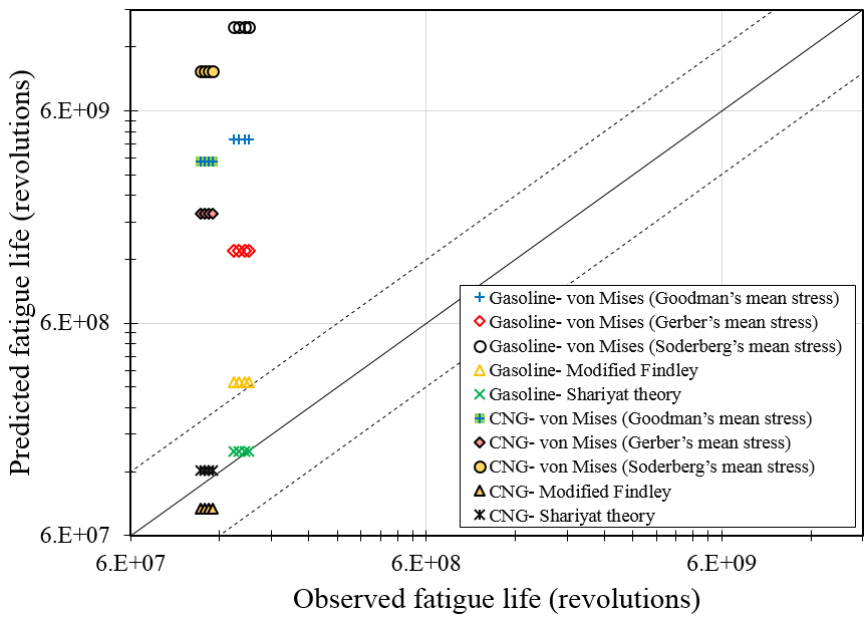


**Figure 19**: Comparison of the observed (experimental) and estimated fatigue lives based on various theories, for the so-called 400 hr durability tests of both the gasoline and CNG engines.

## 6 CONCLUSIONS

In the present research, a systematic performance and fatigue life assessment procedure is presented for the pistons with an emphasis on employing and validating the three-dimensional multiaxial random fatigue criteria recently proposed by the first author. These analyses are crucial e.g. when upgrading a gasoline-based engine to a CNG engine. In this regard, results of the enhanced traditional

theories and the recently proposed theories have been compared with the experimental results for the piston as a typical part with complicated geometry, boundary conditions, and loading conditions. The available HCF criteria have been mainly validated based on simple specimens, and simple boundary and loading conditions. The obtained results for the combustion temperatures and pressures, the temperature distributions, and the fatigue life assessment results obtained by the recently proposed integral-type criterion of the first author, show a good concordance with the experimental results.

## References

Abu-Nada, E., Al-Hinti, I., Al-Sarkhi, A., Akash, B., (2008). Effect of piston friction on the performance of SI engine: A new thermodynamic approach, Journal of Engineering for Gas Turbines and Power 130, Article No. 022802.

Bernasconi, A., Foletti, S., Padopoulos, I.V., (2008). A study on combined torsion and axial load fatigue limit tests with stresses of different frequencies, International Journal of Fatigue 30: 1430–1440.

Borgnakke, C., Sonntag, R.E., (2009). Fundamentals of thermodynamics, 7th Edition, John Wiely & Sons Inc, Hoboken, USA.

Castro, F.C., Araujo, J.A., Mamiya, E.N., Pinheiro, P.A., (2014). Combined resolved shear stresses as an alternative to enclosing geometrical objects as a measure of shear stress amplitude in critical plane approaches. International Journal of Fatigue 66: 161 – 167.

Dowson, D., Taylor, C.M., Yang, L., (1996). Friction modelling for internal combustion engines, Tribology Series 31: 301-318.

Erdman, A., Sandor, G.N., Kota, S., (2001). Mechanism design: Analysis and synthesis, 4th edition, Prentice Hall, New Jersey.

Fatemi, A., Shamsaei, N., (2011). Multiaxial fatigue: An overview and some approximation models for life estimation. International Journal of Fatigue 33 948–958.

Fatemi, A., Socie, D. (1988). A critical plane approach to multiaxial fatigue damage including out-of-phase loading, Fatigue and Fracture of Engineering Materials and Structures 11: 149-166.

Ferguson, P.S., Kirkpatrick, A.T., (2000). Internal combustion engines applied thermosciences, Wiley, New York.

Findley, W.N., (1959). A theory for effect of mean stress on fatigue of metals under combined torsion and axial load or bending, Trans ASME, Journal of Engineering for Industry 1959; 81: 301-306.

Ghazi Mir Saied, S.A., Jazayeri, S.A., Shamekhi, A.H., (2006). Modeling of variable intake valve timing in SI engine, ASME Technical Conference, Internal Combustion Engine Division, Paper No. ICES2006-1411, 789-803.

Heywood, J.B., (1988). Internal combustion engine fundamentals, McGraw-Hill, New York.

Ivashchenko, N.A., Nasyrov, R.A., Timokhin, A.V., (1980). Evaluation of the thermal and stress-strain state of an internal combustion engine piston by the finite element. Problemy Prochnosti 2: 62-67.

Jahanian, O., Jazayeri, S.A., (2009). A comprehensive study on natural gas HCCI engine response to different initial conditions via a thermo-kinetic engine model, ASME Technical Conference, Internal Combustion Engine Division, Paper No. ICEF2009-14084.

Kajiwara, H., Fujioka, Y., Suzuki, T., Negishi, H., (2002). An analytical approach for prediction of piston temperature distribution in diesel engines. JSAE Review 23: 429–34.

Karamangil, M., Kaynakli, O., Surmen, A., (2006). Parametric Investigation of cylinder and jacket side convective heat transfer coefficients of gasoline engines, Energy Conversion Management 47: 800–816.

Konecna, R., Nicoletto, G., Kunz, L., Riva, E., (2015). The role of elevated temperature exposure on structural evolution and fatigue strength of eutectic AlSi12 alloys. doi:10.1016/j.ijfatigue.2015.05.007.

Li, J., Zhang, Z.-P., Sun Q., Li C.-W., (2011). Multiaxial fatigue life prediction for various metallic materials based on the critical plane approach. International Journal of Fatigue 33: 90 – 101.

Lipski, A., Mroziński, S., (2012). The Effects of Temperature on the Strength Properties of Aluminium Alloy 2024-T3. Acta Mechanica et Automatica, 6: 62-66.

MAHLE GmbH, Pistons and engine testing, Chapter 4: Piston materials, Vieweg+Teubner Verlag, Springer, Stuttgart, 2012.

Mohammadi, A., Jazayeri, S.A., Ziabasharhagh, M., (2008). Numerical simulation of convective heat transfer in a spark ignition engine, ASME Technical Conference, Internal Combustion Engine Division, Paper No. ICES2008-1687.

Papuga, J., (2011). A survey on evaluating the fatigue limit under multiaxial loading. International Journal of Fatigue 33: 153 – 165.

Ramos, J., (1989). Internal Combustion Engine Modelling, Taylor & Francis, New York.

Schijve, J., (2009). Fatigue of Structures and Materials, Second Edition, Springer, Germany.

Scholz, B., Bargende, M., (2000). Three-dimensional simulation of the piston group, SAE technical paper No. 2000-01-1239.

Shahangian, S.N., Jazayeri, S.A., Bagheri, N., (2007). Study on characteristics of HCCI engine operation for EGR, equivalence ratio and intake charge temperature and pressure while using dimethyl ether, ASME Technical Conference, Internal Combustion Engine Division, Paper No. ICEF2007-1644, 127-137.

Shariyat, M., (2008). A fatigue model developed by modification of Gough's theory, for random non-proportional loading conditions and three-dimensional stress fields, International Journal of Fatigue 30: 1248-1258.

Shariyat, M., (2009a). Two new multiaxial HCF criteria based on virtual stress amplitude and virtual mean stress concepts, for complicated geometries and random non-proportional loading conditions, Transactions of ASME, Journal of Engineering Materials and Technology 131: 031014 (1-13).

Shariyat, M., (2009b). Three energy-based multiaxial HCF criteria for fatigue life determination in components under random non-proportional stress fields, Fatigue and Fracture of Engineering Materials and Structures 32: 785-808.

Shariyat, M., (2010). New multiaxial HCF criteria based on instantaneous fatigue damage tracing in components with complicated geometries and random non-proportional loading conditions, International Journal of Damage Mechanics 19: 659-690.

Shariyat, M., Djamshidi, P., (2009). Minimizing the engine-induced harshness based on the DOE method and sensitivity analysis of the full vehicle NVH model, International Journal of Automotive Technology 10: 687-696.

Silva, F.S., (2006). Fatigue on engine pistons, A compendium of case studies, Engineering Failure Analysis 13: 480–492.

Smith, K., Topper, T. H., Watson, P., (1970). A stress-strain function for the fatigue of metals. Journal of materials 5: 767-778.

Socie, D., (1987). Multiaxial fatigue damage models. Journal of Engineering Materials and Technology 109: 293-298.

Socie, D.F., Marquis, G.B., (2000). Multiaxial fatigue, SAE International.

Su, X., Zubeck, M., Lasecki, J., Engler-Pinto Jr, C., Tang, C., Sehitoglu, H., Allison, J., (2002). Thermal fatigue analysis of cast aluminum cylinder heads, SAE technical paper No. 2002-01-0657.

Thring, R.H., (1992). Engine friction modeling, SAE Technical paper No. 920482.

Tung, S.C., McMillan, M.L., (2004). Automotive tribology overview of current advances and challenges for the future, Tribology International 37: 517–536.

Valdés, M., Casanova, J., Rovira, A., Trinidad, M., (2001). Design of carbon pistons using transient heat transfer and stress analyses, SAE technical paper No. 2001-01-3217.

Woschni, G., (1967). Universally applicable equation for the instantaneous heat transfer coefficient in internal combustion engine, SAE Paper No. 670931.